polysaccharides

MDPI

Article

Chemically Modified Alginate Derivatives: From Water Processable Systems to Water Resistant Functional Matrices

Gabriel Lombardo [1,2], Joana E. Tasque [1], Margot Nadler [1,3], Chiara Llanes [1], Renata Giovanna Fauceglia [1], Andrés G. Salvay [4], Ezequiel Rossi [1,2,*] and Maria Ines Errea [1,2,*]

1 Instituto Tecnológico de Buenos Aires (ITBA), Lavardén 315, Ciudad Autónoma de Buenos Aires C1437FBG, Argentina; glombardo@itba.edu.ar (G.L.); jtasque@itba.edu.ar (J.E.T.); nadler@insa-toulouse.fr (M.N.); cllanes@itba.edu.ar (C.L.); rfauceglia@itba.edu.ar (R.G.F.)
2 Consejo Nacional de Investigaciones Científicas y Técnicas (CONICET), Godoy Cruz 2290, Ciudad Autónoma de Buenos Aires C1425FQB, Argentina
3 The National Institute of Applied Sciences of Toulouse (INSA-Toulouse), 135 Avenue de Rangueil, 31077 Toulouse, Cedex 4, France
4 Departamento de Ciencia y Tecnología, Universidad Nacional de Quilmes, Bernal B1876, Argentina; asalvay@unq.edu.ar
* Correspondence: ezrossi@itba.edu.ar (E.R.); merrea@itba.edu.ar (M.I.E.)

Abstract

Amidation is widely used to tailor alginate properties, yet different carbodiimide-mediated coupling procedures have been reported without establishing whether the reaction sequence affects the resulting materials. Here, this methodological gap was addressed by modifying sodium alginate with 1,4-butanediamine, 1,6-hexanediamine, and cystamine using two alternative reaction sequences. Both routes produced materials with comparable structural and physicochemical properties, demonstrating that, under the conditions studied, the reaction outcome was not significantly affected by the order of reagent addition. Beyond this methodological finding, the resulting derivatives exhibited a distinctive combination of aqueous processability and water stability: alkaline treatment followed by neutralization yielded homogeneous aqueous systems, whereas subsequent drying produced water-insoluble films. This behavior enables functional additives to be incorporated during aqueous processing while providing stable matrices upon water exposure. To demonstrate the technological relevance of these properties, the materials were evaluated as seed coatings using *Vigna radiata* as a model system. The 1,6-hexanediamine derivative showed the highest persistence under simulated rainfall without impairing germination, while Zn incorporation demonstrated the ability of the coating to act as a micronutrient carrier. Overall, these findings provide new insights into alginate amidation and establish a versatile route toward water-processable, water-stable functional coatings.

Keywords: functional alginate derivatives; water insoluble matrices; aqueous processability

Check for updates

Academic Editor: Artur Valente

Received: 31 July 2026
Revised: 25 August 2026
Accepted: 31 August 2026
Published: 3 September 2026

Copyright: © 2026 by the authors. Licensee MDPI, Basel, Switzerland. This article is an open access article distributed under the terms and conditions of the Creative Commons Attribution (CC BY) license.

1. Introduction

Sodium alginate is a naturally occurring polysaccharide primarily extracted from brown seaweeds such as *Laminaria*, *Macrocystis*, and *Ascophyllum*, which are abundant in cold and temperate coastal regions, including the North Atlantic, North Pacific, and parts of the Southern Hemisphere [1]. As a marine-derived resource, alginate represents a renewable and sustainable raw material that does not compete with agricultural land required for food production, making it an attractive feedstock for the development of

sustainable bio-based materials. It is widely recognized for its biocompatibility, low toxicity, and biodegradability, which has enabled its extensive use in biomedical, pharmaceutical, agriculture and food-related applications [2–7]. Structurally, it is an anionic copolymer composed of β-D-mannuronic (M) and α-L-guluronic (G) acid residues arranged in varying block sequences (Figure 1) [8,9], which strongly influence its physicochemical behavior [10]. Like all polysaccharides, alginate contains abundant hydroxyl groups that can be chemically modified, while the additional presence of carboxyl groups along its backbone broadens the range of accessible functionalization strategies, allowing fine control over properties such as solubility, hydrophilicity, and mechanical stability [11].

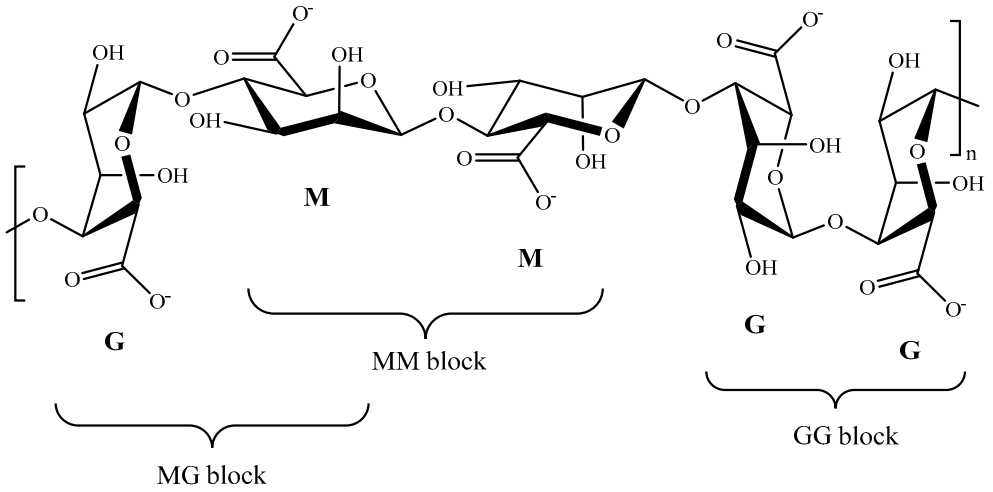


Figure 1. Schematic representation of alginate structure illustrating an average distribution of mannuronic (M) and guluronic (G) units.

Chemical functionalization of alginate has been widely explored through reactions targeting its functional groups, including esterification, phosphorylation, oxidation, sulfation, and amidation [12–15]. Among these strategies, amide bond formation is particularly attractive due to its high hydrolytic stability and robustness under a wide range of conditions. A widely employed approach for alginate amidation involves activation of its carboxyl groups with 1-ethyl-3-(3-dimethylaminopropyl)carbodiimide (EDC), commonly in the presence of *N*-hydroxysuccinimide (NHS) [16,17]. However, different reaction sequences have been reported: in some studies, alginate is first activated with EDC/NHS before addition of the amine, whereas in others the amine is mixed with alginate prior to addition of the activation system [16–24]. Despite the use of both procedures, their direct comparison under equivalent reaction conditions has not been reported, leaving the influence of reagent addition order on the resulting materials unresolved.

Beyond the reaction sequence, the use of diamines introduces additional structural complexity, as they can react through a single amino group, leaving a pendant free amine, or through both amino groups, leading to covalent crosslinking of alginate chains, while a fraction of the original carboxyl groups may remain unreacted. However, considerably fewer studies have explored alginate amidation with diamines [16–18,25], and the relative proportions of these different structures have not been quantitatively established.

Thus, to the best of our knowledge, neither the influence of the EDC/NHS reaction sequence nor the quantitative distribution of the structures generated upon diamine incorporation has been systematically addressed.

In this context, alginate was modified with three structurally distinct diamines: 1,4-butanediamine, 1,6-hexanediamine, and cystamine. Two EDC/NHS-mediated reaction sequences differing in the order of reagent addition were directly compared, and the resulting

derivatives were chemically characterized to determine the relative proportions of unmodified, monosubstituted, and crosslinked structures. The selection of 1,4-butanediamine and 1,6-hexanediamine allowed the influence of hydrocarbon chain length on the physicochemical properties of the resulting materials to be investigated, whereas cystamine introduced a disulfide bond with potential redox-responsive behavior [26–29].

Beyond the influence of diamine structure on the physicochemical properties of the resulting materials, a particularly interesting feature of these derivatives emerged during their evaluation. Although insoluble under neutral conditions, they could be transformed into homogeneous aqueous systems through alkaline treatment followed by neutralization, enabling subsequent processing. Drying of these solutions yielded films that remained insoluble upon re-exposure to water while enabling the retention of incorporated additives.

This combination of properties may be attractive for the development of materials intended to operate under humid or aqueous conditions. From a practical perspective, it enables the preparation of formulations in water followed by the formation of water-resistant films after drying, a feature commonly exploited in many coating technologies [30–32]. In addition, the ability to incorporate functional additives during processing and subsequently retain them within the resulting matrix further expands the potential utility of these materials [33]. Achieving such functionality with a renewable polysaccharide-based system is particularly attractive in view of the growing demand for more sustainable materials.

As a proof-of-concept, the potential of the modified alginate derivatives to act as water-processable carriers for functional additives was evaluated using seed coating as a model application [34–36]. Mung bean (*Vigna radiata*) seeds were first used to assess the ability of the materials to form continuous and uniform layers on the seed surface. The persistence of the resulting coatings under wet conditions was subsequently investigated through a simulated rainfall assay, allowing the identification of the formulation that best preserved coating integrity after water exposure. The compatibility of this coating with seed germination and early seedling development was also evaluated. Finally, Zn was incorporated into the selected formulation as a model micronutrient to demonstrate the incorporation of functional additives during processing [37–39]. Germination experiments followed by Zn determination in the resulting seedlings were performed to assess the transfer of the incorporated micronutrient from the coating to the plant system and thereby validate the effectiveness of the material as a carrier for functional additives.

2. Materials and Methods

2.1. Materials

Sodium alginate (Prod. No. 180947; 13.5% water content), 1,4-diaminobutane dihydrochloride (BDA), hexamethylenediamine dihydrochloride (HDA), cystamine dihydrochloride (CYS), 5,5′-dithiobis(2-nitrobenzoic acid) (DTNB), zinc nitrate and sodium carboxymethyl cellulose (CMC) (Mw ~ 250,000, degree of substitution: 1.2) were purchased from Sigma-Aldrich (Saint Louis, MO, USA). Sodium borohydride was obtained from Dorwil (Martínez, Buenos Aires, Argentina). Monopotassium phosphate and dipotassium phosphate were obtained from Anedra (Los Troncos del Talar, Buenos Aires, Argentina). Phosphoric acid, hydrochloric acid, potassium hydroxide and sodium hydroxide were obtained from Merck (Burlington, MA, USA). *N*-hydroxysuccinimide (NHS) and *N*-ethyl-N′-(3-dimethylaminopropyl) carbodiimide hydrochloride (EDC) (reagent grade) were purchased from BLD Pharmatech Ltd. (Songjiang District, Shanghai, China). All other reagents were of analytical grade and used as received.

2.2. Chemical Modifications of Sodium Alginate

Amide-linked alginate derivatives were synthesized via carbodiimide-mediated coupling, involving activation of alginate carboxyl groups with EDC/NHS followed by reaction with diamines [16,17,21]. Two different protocols were employed, differing in the sequence of addition of the coupling agents and the diamine.

Condition 1: Activation of alginate prior to diamine addition

Sodium alginate (372 mg, corresponding to 1.88 mmol of carboxyl groups) was dissolved in distilled water (25 mL) under mechanical stirring (500 rpm). The solution was cooled in an ice bath, and the pH was adjusted to 7 using 0.1 M NaOH. A freshly prepared aqueous solution of EDC (1.80 g, 9.39 mmol) and NHS (1.08 g, 9.39 mmol) (3 mL) was then added to activate the carboxyl groups. After 30 min, a solution of the corresponding diamine hydrochloride (1,4-butanediamine (BDA, 151 mg), 1,6-hexanediamine (HDA, 178 mg), or cystamine (CYS, 211 mg), equivalent to 1.88 mmol of amino groups) in cold water (2 mL) was introduced into the reaction mixture.

The reaction was maintained under stirring in an ice bath for 6.5 h and subsequently allowed to proceed at 4 °C without stirring for 17 h. Then it was quenched by addition of 10% NaOH (5 mL). The resulting products (AlgBDA-1, AlgHDA-1, and AlgCYS-1) were purified by dialysis (MWCO 6–8 kDa) and freeze-dried, yielding 577 mg, 660 mg, and 650 mg, respectively.

Condition 2: Diamine addition prior to carbodiimide activation

Using the same reagent quantities described above, sodium alginate was dissolved in distilled water, and the corresponding diamine hydrochloride (BDA, HDA, or CYS) was added prior to activation. The pH was adjusted to 7 with 0.1 M NaOH, and the mixture was cooled in an ice bath. Subsequently, EDC and NHS were added to initiate in situ activation of the carboxyl groups in the presence of the diamine.

The reaction was stirred in the ice bath for 7 h and then maintained at 4 °C without stirring for 17 h. Quenching, purification, and drying steps were carried out as described above, yielding AlgBDA-2, AlgHDA-2, and AlgCYS-2 (576 mg, 652 mg, and 684 mg, respectively).

2.3. Chemical Characterization

2.3.1. Spectroscopic Studies

Fourier Transform Infrared Spectroscopy (FT-IR): Native alginate and its derivatives were characterized using a Thermo Scientific Nicolet 6700 spectrometer (Thermo Fisher Scientific, Waltham, MA, USA). For analysis, each sample was finely ground with KBr (Thermo Spectra-Tech, Madison, WI, USA, *FT*-IR grade, 99+%) and pressed into pellets of approximately 3 mm diameter using a manual press (PIKE Technologies, Madison, WI, USA). Spectra were recorded in the 400–4000 cm^{-1} range, with a resolution of 4 cm^{-1} and accumulation of 32 scans per sample.

2.3.2. Evaluation of Disulfide Incorporation and Redox Responsiveness

The free thiol content of AlgCYS-1 and AlgCYS-2 was first quantified using Ellman's assay [40–42] to establish the baseline thiol content prior to reduction. Briefly, samples (5.0 mg) were dispersed in distilled water (10 mL), followed by the addition of phosphate buffer (0.5 M, pH 8.0, 15 mL). Ellman's reagent (DTNB, 0.03%, 25 mL) was then introduced, and the absorbance was measured at 412 nm after 1 h. A calibration curve was constructed using cysteine standard solutions in the range of 5–30 ppm.

To determine the disulfide content and assess the susceptibility of the incorporated disulfide bonds to reductive cleavage, the samples were subsequently subjected to reduction with $NaBH_4$. Samples (5.0 mg) were treated with 1% $NaBH_4$ solution (6 mL) under stirring

overnight. Excess reducing agent was subsequently quenched by addition of 1 M HCl (4 mL), followed by incorporation of phosphate buffer (15 mL). Ellman's reagent (25 mL) was then added, and absorbance was recorded at 412 nm after 1 h. The increase in thiol content following reduction was attributed to the cleavage of disulfide bonds, and the disulfide content was calculated from the difference between the thiol concentrations measured before and after reduction.

All measurements were performed in duplicate and results are expressed as mean ± standard deviation.

2.3.3. Determination of Free Amino Groups and Carboxylic Acid Content

The content of free amine and carboxyl groups in the amide-modified alginate derivatives was evaluated by conductometric titration [40,43,44]. Briefly, 300 mg of sample was dispersed in 0.1 M HCl (10.0 mL) under continuous stirring, followed by dilution with distilled water (25 mL). The resulting dispersion was titrated with 0.1 M NaOH, added in 0.05 mL increments. After each addition, both conductivity and pH were recorded using a Sper Scientific Bench-Top Water Quality Meter 86003 (Scottsdale, AZ, USA) equipped with appropriate probes.

Titration curves were obtained by plotting conductivity as a function of the volume of NaOH added. Equivalence points were determined from the intersection of linear regions identified by linear regression. The molar fractions of each structural unit (i.e., x_{COOH}, x_{NH2} and x_{CL}) were determined by solving Equations (1)–(3). In these equations, ΔV_1 and ΔV_2 denotes the volumes of NaOH (L) consumed between the first and second, and the second and third equivalence points, respectively; [NaOH] is the sodium hydroxide concentration (mol L^{-1}), m is the mass of alginate derivative (g), $\overline{Mr}$ represents the molecular weight (g mol^{-1}) of the average monomer unit, and Mr_{COOH}, Mr_{NH2} and Mr_{CL} denotes the molar masses (g mol^{-1}) of the respective structural unit [43,44].

$$x_{COOH} \cdot \frac{m}{\overline{Mr}} = \Delta V_1 \cdot [\text{NaOH}] \quad (1)$$

$$x_{NH2} \cdot \frac{m}{\overline{Mr}} = \Delta V_2 \cdot [\text{NaOH}] \quad (2)$$

$$\overline{Mr} = Mr_{NH2} \cdot x_{NH2} + Mr_{COOH} \cdot x_{COOH} + Mr_{CL} \cdot x_{CL} \quad (3)$$

2.4. Thermogravimetric Analyses (TGA)

The thermal stability of the amide-modified alginate derivatives was evaluated using a TA Instruments Q500 thermogravimetric analyzer (New Castle, DE, USA). Freeze-dried samples (ca. 3 mg) were placed in platinum pans and heated from 40 to 700 °C at a rate of 10 °C min^{-1} under a nitrogen atmosphere (flow rate: 60 mL min^{-1}) [45].

Derivative thermogravimetric (DTG) curves were obtained using TA Universal Analysis software (v4.5, TA Instruments). The temperature corresponding to the maximum degradation rate was determined from the peak of the DTG curve. All measurements were performed in triplicate, and representative curves are presented.

2.5. Water Solubility Tests

The solubility of the materials was evaluated under acidic, neutral, and basic conditions. Briefly, samples (100 mg) were placed in 10 mL of 0.1 M HCl, distilled water, or 0.1 M NaOH under magnetic stirring. After 60 min, the pH of each system was adjusted to 7 using aqueous HCl or NaOH solutions, and the resulting systems were visually inspected to evaluate the solubility behavior of the materials.

Systems that yielded homogeneous solutions after pH adjustment were dried at 60 °C for 24 h to obtain films. The resulting films were subsequently resuspended in distilled water, and their structural integrity was visually assessed.

2.6. Swelling Studies

Dry films were immersed in 50 mL of distilled water and allowed to hydrate for 60 min. Subsequently, the hydrated films were removed from the medium at 30 min intervals, excess surface water was carefully removed using absorbent paper, and the samples were weighed [46]. Two separate films were analyzed for each derivative. For each film, the swelling measurement was repeated through five consecutive hydration–weighing cycles after equilibration, resulting in a total of 10 determinations per derivative. The swelling capacity of the films was calculated according to Equation (4) [47], where $m_{swollen}$ is the weight of the hydrated film and m_{dry} is the weight of the dry film.

$$Swelling = \frac{m_{swollen} - m_{dry}}{m_{dry}} \quad (4)$$

2.7. Seed Treatment of Mung Bean (Vigna radiata)

2.7.1. Preparation of the Coating Formulation

Coating formulations were prepared by dispersing each alginate derivative (50 mg) in 1 mL of 0.1 M KOH. Distilled water (0.3 mL) was subsequently added, and the dispersion was then neutralized with H_2SO_4 (0.2 M, 0.2 mL), followed by the addition of an aqueous carboxymethyl cellulose (CMC, 2% *w*/*v*) solution [48]. Finally, 1 mL of distilled water was added. In the case of AlgHDA, an additional formulation was prepared in which the water aliquot was replaced by 1 mL of a $Zn(NO_3)_2$ solution (1000 ppm Zn). A CMC-based control was prepared following the same protocol but without the alginate derivative. The final composition of each formulation is summarized in Table 1.

Table 1. Composition of coating formulations. CMC: carboxymethyl cellulose; AlgBDA, AlgHDA, and AlgCYS: alginate derivatives obtained with 1,4-butanediamine, 1,6-hexanediamine, and cystamine, respectively; AlgHDA/Zn: Zn-containing AlgHDA formulation.

Treatment	Zn Concentration (ppm)	CMC Concentration (% *w*/*v*)	Alginate Derivative Concentration (% *w*/*v*)
Untreated	-	-	-
CMC	0	1	0
AlgHDA	0	1	1
AlgBDA	0	1	1
AlgCYS	0	1	1
AlgHDA/Zn	200	1	1

2.7.2. Seed Coating

Mung bean (*Vigna radiata*) seeds were treated with a 1% (*v*/*v*) sodium hypochlorite solution for 5 min, thoroughly rinsed six times with distilled water, and dried at 35 °C for 2 h.

For coating, batches of 50 seeds were immersed in the corresponding formulations for 30 s, removed, and dried under a stream of air at 35 °C.

2.8. Scanning Electron Microscopy (SEM) Analysis

SEM (Carl Zeiss Evo 10, ZEISS, Chicago, IL, USA) was used to analyze transverse sections of the seeds. Prior to imaging, the samples were sputter-coated with gold using an ion sputter coater to ensure adequate electrical conductivity. For AlgHDA/Zn-coated

seeds, energy-dispersive X-ray spectroscopy (EDS) (Ultim Max 40, Oxford Instruments, High Wycombe, Buckinghamshire, UK) was additionally performed at selected points of the coating layer and the natural seed coat to evaluate the presence of Zn.

2.9. Rainfall Simulation Test

A simulated rainfall assay was performed using a cylindrical chamber (68 mm diameter) containing pre-moistened glass beads (500–800 µm), which provided a porous medium allowing water to reach the seeds by percolation. For each treatment, twenty seeds were placed between two 3 cm layers of glass beads. Simulated rainfall equivalent to 50 mm of precipitation was applied over a period of 10 min [49,50].

2.10. Seed Germination Assays

Germination tests were performed by placing ten seeds per treatment in 120 mm Petri dishes on moistened filter paper (5 mL of Milli-Q water). All tests were carried out in quadruplicate.

The plates were incubated in the dark at 25 °C, and germination was recorded daily for 5 days [51]. Seeds were considered germinated when the radicle length exceeded 2 mm [52]. On day 5, the seedlings were weighed, and radicle and hypocotyl lengths were measured, followed by drying at 60 °C for 48 h to determine dry weight.

2.10.1. Germination Parameters

The germination percentage (*GP*, %) was calculated after 5 days using the expression of Equation (5) [51].

$$GP(\%) = \frac{Number\ of\ germinated\ seeds}{Total\ number\ of\ seeds} \times 100 \quad (5)$$

The germination energy (*GE*, %) was calculated using the number of germinated seeds recorded after 48 h, according to Equation (6).

$$GE(\%) = \frac{Number\ of\ germinatd\ seed\ after\ 48\ h}{Total\ number\ of\ seeds} \times 100 \quad (6)$$

The germination rate (*GR*, % day^{-1}) and mean germination time (*MGT*, day) were calculated according to Equations (7) and (8) respectively [51].

$$GR = \sum \frac{G_i}{t_i} \quad (7)$$

$$MGT = \frac{\sum(n_i \times t_i)}{\sum n_i} \quad (8)$$

where G_i is the percentage of germinated seeds at time t_i, and n_i is the number of seeds germinated at time t_i.

Finally, the vigor index (*VI*) was calculated according to Equation (9) [51].

$$VI = (mean\ radicle\ length + mean\ hypocotyl\ length) \times GP \quad (9)$$

2.10.2. Determination of Zn Content of the Seedlings

Digestion of dry seedlings was carried out according to the EPA 3050 method [53]. The natural seed coats, which detached from the seedlings during germination, were excluded from the samples prior to drying and digestion. Briefly, samples were placed in digestion tubes and mixed with 5 mL of HNO_3. The mixture was heated at 95 °C for 10 min and then allowed to cool to room temperature. Subsequently, 2.5 mL of HNO_3 was added, and

the samples were heated again at 95 °C for 2 h. After cooling, 1 mL of distilled water and 1.5 mL of H_2O_2 were added, followed by further heating at 95 °C for 2 h.

After cooling, 2.5 mL of HCl and 5 mL of distilled water were added. The samples were reheated at 95 °C for 5 min, allowed to cool, and then diluted to 25 mL with distilled water in volumetric flasks.

Zinc concentration was determined by flame atomic absorption spectrometry (FAAS) with air-acetylene flame, using a Thermo Scientific iCE 3000 instrument (Thermo Fisher Scientific Inc., Cambridge, UK). Zn (II) standard solutions were prepared from 1000 mg L^{-1} Zn stock standard solution (Merck).

2.10.3. Statistical Analysis

All experiments were performed in quadruplicate, and results are reported as mean ± standard deviation unless otherwise indicated. Differences among treatments were initially explored using one-way analysis of variance (ANOVA) [54]. All statistical analyses were performed using R software (version 4.5.2).

3. Results and Discussion

3.1. Chemical Modification of Sodium Alginate

Native alginate was modified with 1,4-butanediamine (BDA), 1,6-hexanediamine (HDA), and cystamine (CYS) through carbodiimide-mediated amidation of its carboxyl groups. As discussed in the Introduction, the use of BDA and HDA allowed the effect of hydrocarbon chain length on the properties of the resulting materials to be investigated, whereas CYS introduced a disulfide bond with potential redox-responsive behavior. Owing to the bifunctional nature of the modifying agents, their incorporation can result in both monosubstituted and covalently crosslinked structures, as illustrated in Figure 2.

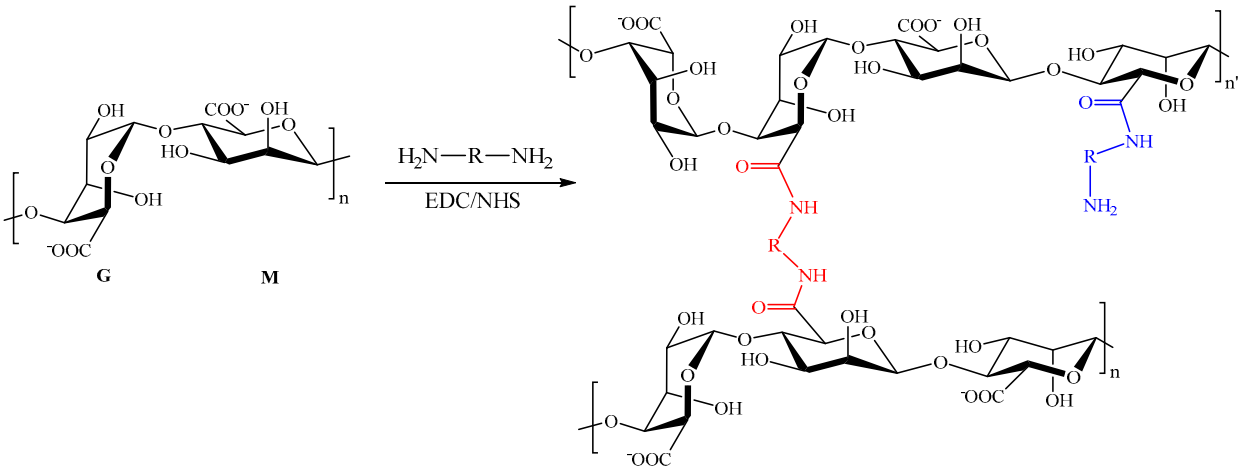


Figure 2. Schematic representation of alginate modification with diamines via amide bond formation using *N*-ethyl-N′-(3-dimethylaminopropyl) carbodiimide hydrochloride (EDC) and *N*-hydroxysuccinimide (NHS) as coupling system.

The influence of the EDC/NHS reaction sequence was evaluated by applying the two procedures reported in the literature to each of the three diamines [16,17,21,22]. In Condition 1, EDC was added prior to the diamine, whereas in Condition 2, EDC was introduced after the diamine.

After freeze-drying, all materials were found to be insoluble in water and their chemical structure was subsequently characterized by Fourier transform infrared spectroscopy (*FT*-IR) and conductometric titration.

The *FT*-IR spectra of the samples as obtained after the reaction are shown in Figure 3a–c.

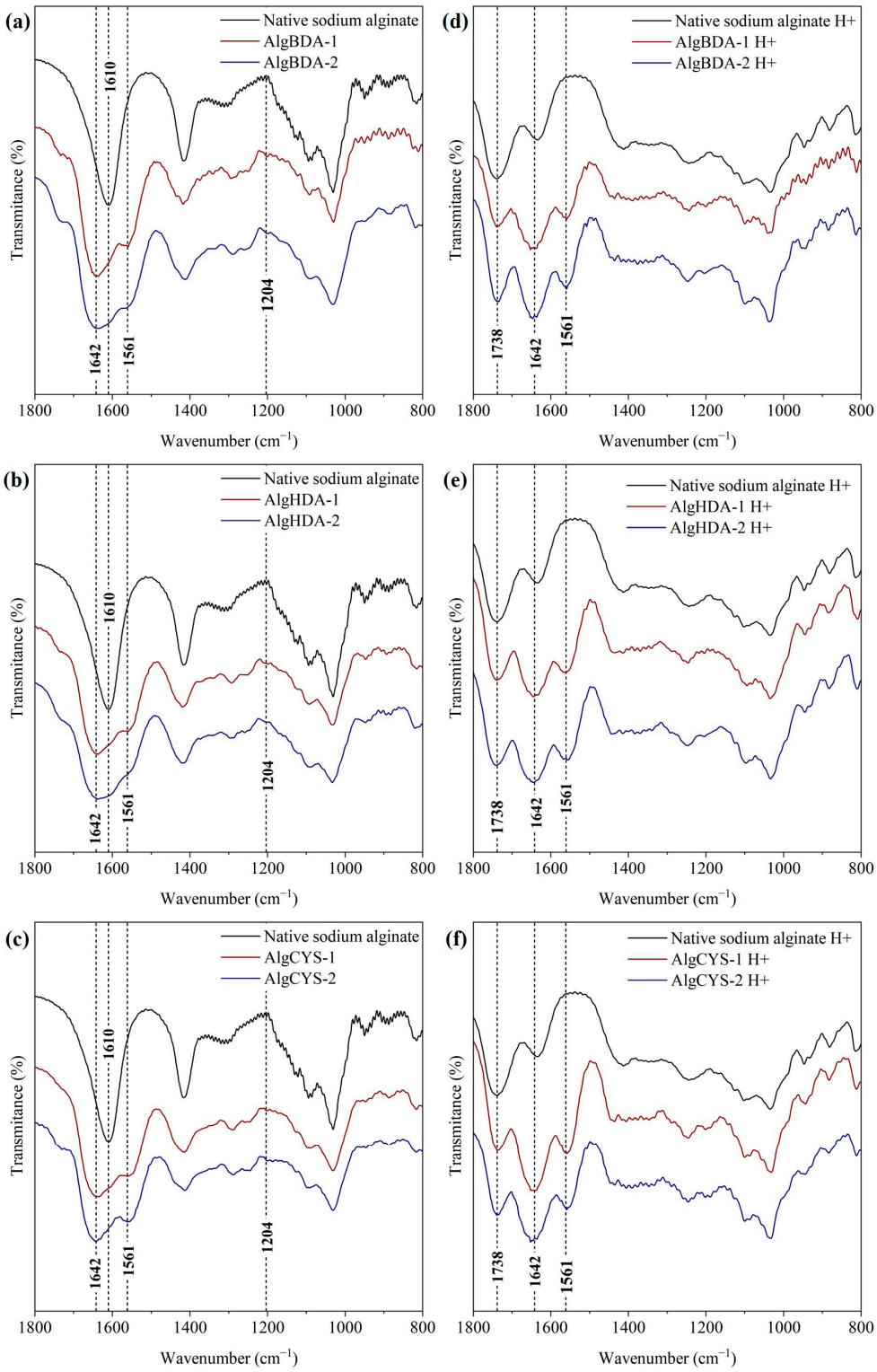


Figure 3. Fourier Transform Infrared (*FT*-IR) spectra of sodium alginate and its derivatives: (**a–c**) samples as obtained after the reaction and (**d–f**) samples after acidification process. Suffixes 1 and 2 denote synthesis conditions 1 and 2, respectively.

The *FT*-IR spectra of all modified alginate derivatives displayed new bands at 1642, 1561, and ~1200 cm^{-1} that were absent in native alginate. These bands are attributed to the amide I (C=O stretching), amide II (N–H bending coupled with C–N stretching), and C–N

stretching vibrations of newly formed secondary amide groups, respectively, providing strong evidence for the formation of amide linkages [14,17,22,25,43,55–58]. The spectra of the modified derivatives also exhibited a shoulder at approximately 1735 cm^{-1}, assigned to the C=O stretching vibration of partially protonated carboxylic acid groups [40]. It should be noted, however, that the bands observed at 1642 and 1561 cm^{-1} are partially superimposed on the broad carboxylate absorption region, particularly the asymmetric COO^- stretching band centered around 1610 cm^{-1}, which hinders their complete resolution. To enhance band resolution, the samples were acidified, freeze-dried, and subsequently reanalyzed by *FT*-IR (Figure 3d–f). Under these conditions, conversion of carboxylate groups into carboxylic acid groups results in a more distinct band at ~1735 cm^{-1}, enabling clearer differentiation from the amide signals [44].

For the cystamine derivatives, it was also important to establish whether the disulfide bond was preserved following alginate modification and retained its susceptibility to reductive cleavage. Free thiol groups were therefore quantified in AlgCYS derivatives before and after treatment with sodium borohydride. No detectable thiol groups were found before reduction, whereas the reducing treatment generated 740 ± 70 µmol g^{-1} of thiol groups. The appearance of thiol groups upon reduction confirms that cystamine-derived disulfide bonds were preserved following incorporation into the alginate matrix and, importantly, remained susceptible to cleavage under reducing conditions. Thus, this experiment provides a simple proof of the redox-responsive behavior conferred by cystamine incorporation.

On the other hand, as discussed above, the reaction of alginate with diamines can lead to the formation of both mono-substituted units and covalently crosslinked structures. The possible structural units are schematically illustrated in Figure 4.

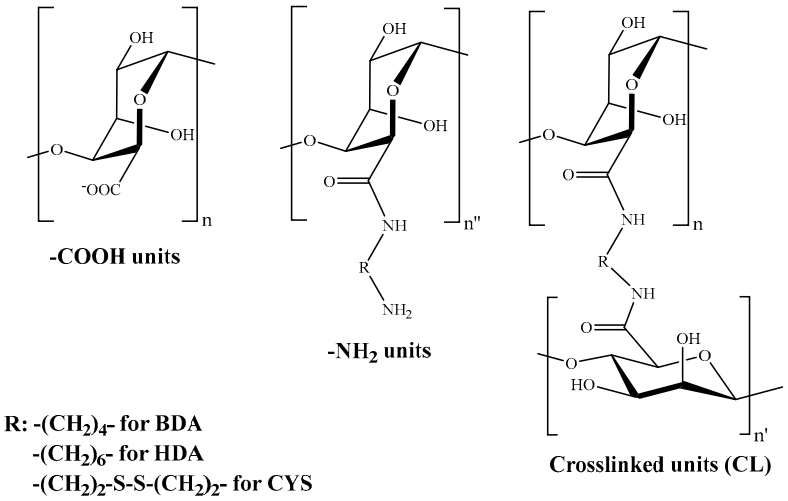


Figure 4. Schematic representation of possible structural units in amide-containing alginate derivatives with 1,4-butanediamine (BDA), 1,6-hexanediamine (HDA) and cystamine (CYS). The location of the modification on guluronic or mannuronic residues is shown for illustrative purposes only and does not imply preferential functionalization of either unit.

The relative content of each structural unit (i.e., –COOH, $–NH_2$, and CL) in the different materials, determined by conductometric titration, is summarized in Table 2. As shown in the table, materials prepared using either activation sequence exhibited very similar compositions, with comparable proportions of carboxylic acid, amine, and crosslinked units. Accordingly, no significant differences between the two EDC activation sequences were detected by either *FT*-IR or conductometric titration.

Table 2. Structural units elucidated by conductometric titration for the alginate derivatives.

Material	-COOH Units (%)	-NH_2 Units (%)	Crosslinked Units (%)
AlgBDA-1	38 ± 2	33 ± 2	29 ± 3
AlgBDA-2	39 ± 2	29 ± 2	32 ± 3
AlgHDA-1	51 ± 2	33 ± 2	16 ± 3
AlgHDA-2	48 ± 2	33 ± 2	19 ± 3
AlgCYS-1	45 ± 2	36 ± 2	19 ± 3
AlgCYS-2	47 ± 2	34 ± 2	19 ± 3

Thermogravimetric analyses were carried out to assess the thermal behavior of native sodium alginate and its amide derivatives (Figure 5). Both native sodium alginate and the modified samples exhibited a main decomposition event at approximately 240 °C [59,60].

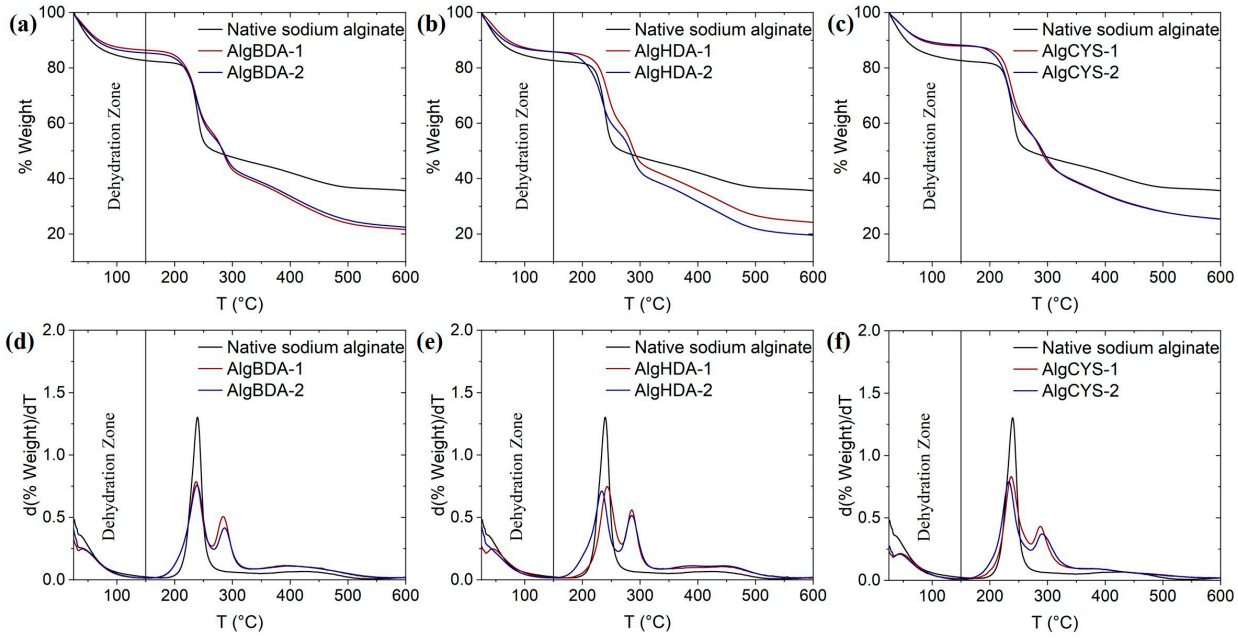


Figure 5. Thermogravimetric (TGA) analysis of freeze-dried sodium alginate and its amide derivatives. Weight loss as a function of temperature is shown for sodium alginate and the AlgBDA (**a**), AlgHDA (**b**), and AlgCYS (**c**) derivatives obtained under conditions 1 and 2. The corresponding derivative thermogravimetric (DTG) curves are presented in panels (**d**), (**e**), and (**f**), respectively.

In the modified samples, the characteristic degradation peak of native alginate was observed to split into two distinct events, with a second peak emerging at a higher temperature, between 284 and 291 °C. The appearance of this additional degradation event indicates the formation of structures with enhanced thermal stability, which may be associated with an increased degree of crosslinking [40,61].

For each derivative, the samples obtained under conditions 1 and 2 exhibited comparable TGA and DTG profiles. Although minor differences in mass loss and peak intensities were observed, no substantial changes in the degradation pattern or the appearance of additional thermal events were detected. These results suggest that the two synthesis conditions did not lead to markedly different products.

Overall, the characterization results provide no evidence that the order of reagent addition during carbodiimide-mediated coupling affects the nature of the final products. The two activation sequences therefore appear to be equivalent under the conditions

investigated. Accordingly, materials prepared under Condition 1 were selected for all subsequent studies as a representative system.

3.2. Solubility Assays

Since processability in aqueous media is a key aspect of the present work, the solubility behavior of the three modified alginate derivatives was investigated in greater detail. Under acidic and neutral conditions, all derivatives remained insoluble and formed hydrated gel-like structures. Upon increasing the pH, a substantial increase in solubilization was observed; however, residual turbidity indicated that complete dissolution was not achieved. Interestingly, when the systems initially dispersed under basic conditions were subsequently neutralized, complete solubilization of the materials was observed (Figure 6). This behavior was consistently reproduced in five independent experiments, confirming the robustness of the response.

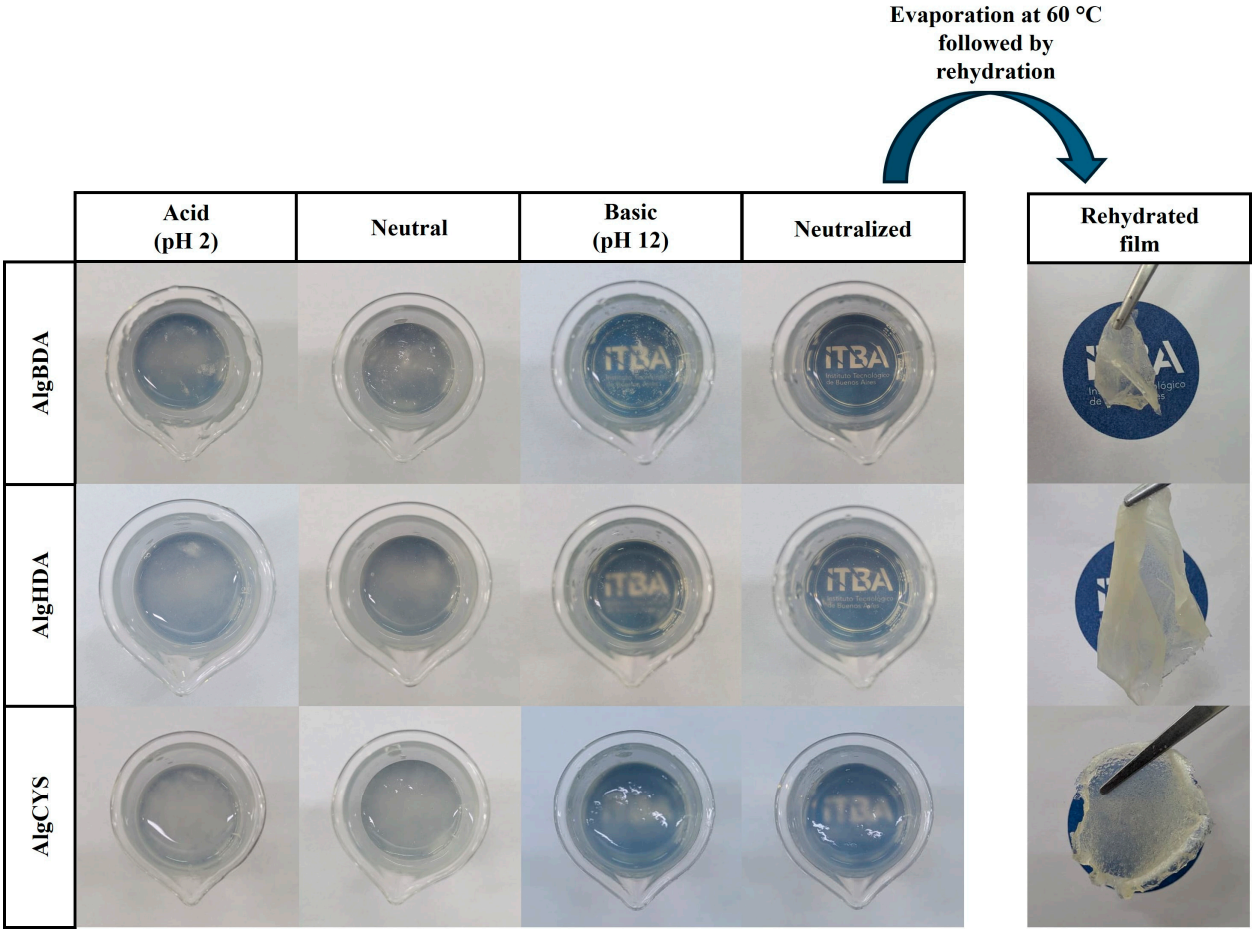


Figure 6. Solubility behavior of AlgBDA, AlgHDA, and AlgCYS under acidic, neutral, and basic conditions. The column labeled "Neutralization" corresponds to samples that were initially dispersed under basic conditions and subsequently adjusted to pH 7. The resulting solutions were dried at 60 °C to obtain films, which were then rehydrated in water. Representative images of the rehydrated films are shown in the right panel.

An even more remarkable finding was that drying the resulting solutions at 60 °C produced films that remained insoluble upon resuspension in water at neutral pH (Figure 6). As discussed in the Introduction section, this behavior is particularly attractive because it enables processing in aqueous media, thereby facilitating the incorporation of functional additives during formulation, followed by the formation of water-insoluble matrices after drying.

Such a combination of processability and subsequent insolubility may be advantageous for applications requiring the retention of incorporated functionalities under aqueous conditions.

3.3. Swelling Studies

Swelling studies were performed on the films, and the results are shown in Figure 7. The three systems exhibited significantly different swelling values (Tukey's HSD post-hoc test, $p \leq 0.05$). The AlgBDA derivative showed a considerably higher swelling degree compared to the other two systems, which is consistent with its lower relative hydrophobicity within the series. Among the remaining samples, AlgCYS exhibited the lowest swelling capacity, as expected due to its higher hydrophobic character associated with the presence of sulfur-containing cystamine groups [62].

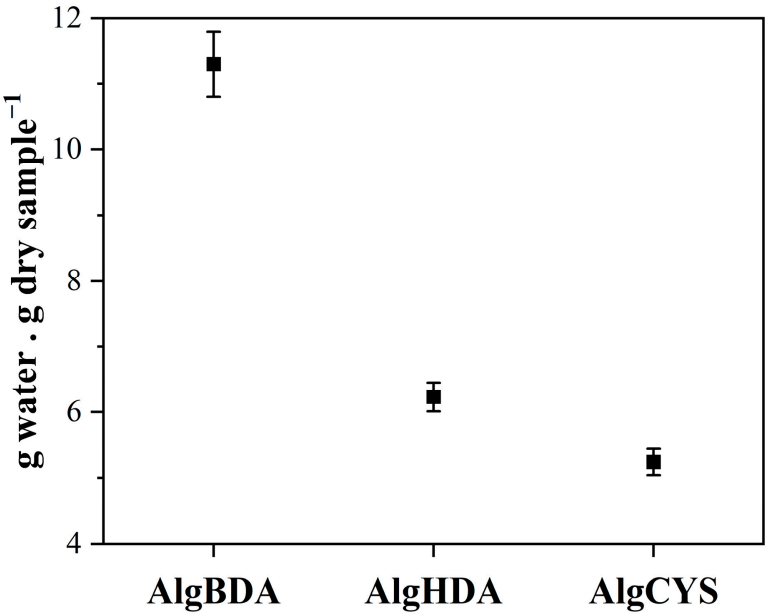


Figure 7. Water absorption capacity of the AlgBDA, AlgHDA, and AlgCYS derivatives. Values are expressed as grams of water absorbed per gram of dry sample, and error bars represent the 95% confidence intervals of the mean from ten determinations for each derivative. Significant differences among samples were observed (one-way ANOVA followed by Tukey's HSD test, $p \leq 0.05$).

3.4. Seed Coating

To demonstrate the practical utility of the developed materials, seed coating was selected as a model application. This system takes advantage of the ability to process the materials in aqueous media while forming water-insoluble coatings upon drying. The study was designed to assess the feasibility of this approach under representative conditions.

A CMC-only formulation was included as a control, since CMC was present in all developed systems [48,63,64]. This allowed the specific contribution of the amide-modified alginate derivatives to be distinguished from that of the polysaccharide matrix.

Mung bean (*Vigna radiata*) seeds were coated with the different formulations and analyzed by SEM to evaluate coating formation. Representative cross-sectional micrographs are shown in Figure 8.

In coated seeds, a continuous outer film was observed across all formulations, confirming successful coating formation. The CMC coating formed a relatively thin layer (1–3 μm), whereas AlgCYS-, AlgBDA-, and AlgHDA-based coatings exhibited thicker layers, ranging from 4 to 8 μm.

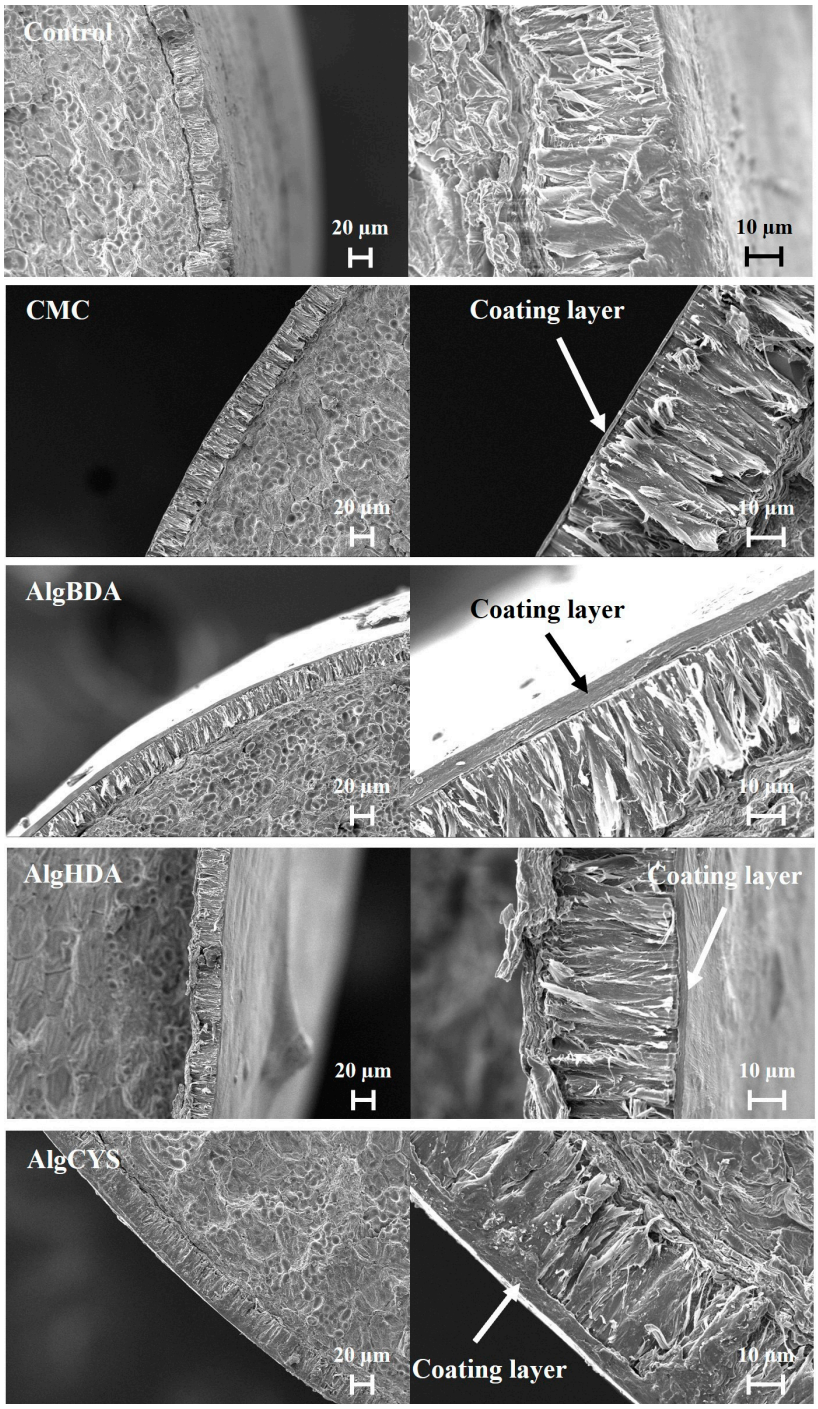


Figure 8. Scanning electron microscopy (SEM) micrographs of cross sections of mung bean seeds after the different treatments, recorded at 500× (left) and 2500× (right) magnification. Treatments included untreated seeds (control), seeds coated with a CMC-only formulation, and seeds coated with formulations containing the modified alginate derivatives. Arrows indicate the coating layer.

3.5. Evaluation of Coating Stability Under Simulation Rainfall

The water-insolubility of the films suggested that the developed materials could potentially provide enhanced resistance to coating removal under wet conditions. As a preliminary assessment of this possibility, coated seeds were subjected to a simulated rainfall assay as was described in the Section 2. The morphology of the coatings after water exposure was subsequently examined by SEM (Figure 9).

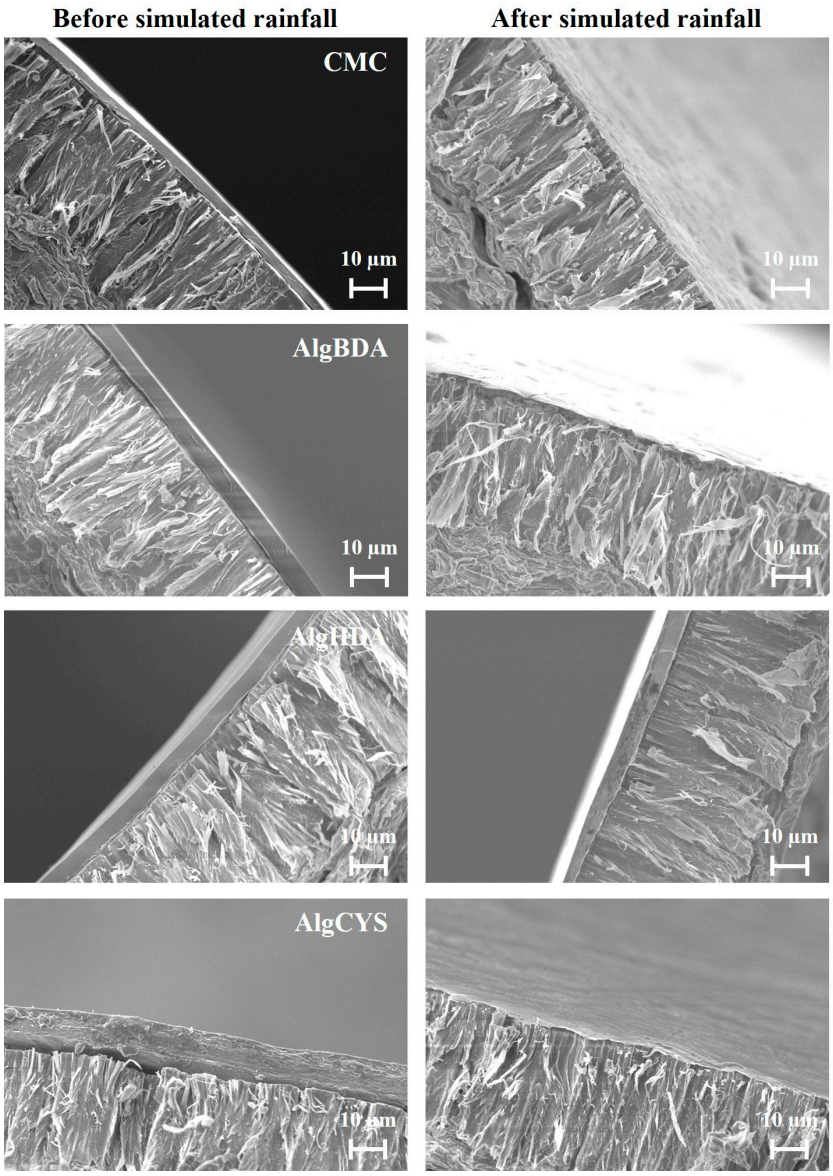


Figure 9. Cross-sectional SEM micrographs of coated seeds acquired at 2500× magnification. Images in the left column correspond to seeds not subjected to the simulated rainfall assay, whereas those in the right column correspond to seeds after the simulated rainfall assay. From top to bottom: CMC, AlgBDA, AlgHDA, and AlgCYS coatings.

Marked differences in coating persistence were observed after the simulated rainfall assay. For seeds coated with CMC, the coating layer was no longer clearly distinguishable, indicating extensive coating loss. A similar behavior was observed for AlgBDA- and AlgCYS-coated seeds, where the surface layer was largely absent after water exposure. In contrast, seeds coated with AlgHDA retained a well-defined outer layer following the rainfall treatment, with no apparent changes in coating morphology compared to the corresponding samples before water exposure. These results demonstrate that AlgHDA provides complete resistance to coating removal under simulated rainfall conditions, highlighting its suitability for applications requiring high water stability. This characteristic may represent an advantage in seed coating applications, where intense rainfall shortly after sowing can contribute to coating removal and the loss of incorporated active components.

Based on the above results, AlgHDA was selected for further evaluation.

3.6. Seed Germination Assays

Since seed coatings must remain compatible with germination and early seedling development, germination assays were performed using mung bean seeds coated with the AlgHDA formulation. Untreated seeds and seeds coated with a CMC-only formulation were included as controls. The resulting germination parameters are summarized in Table 3.

Table 3. Germination indices of Mung bean (*Vigna radiata*) seeds under different coating conditions. Values are expressed as mean ± standard deviation (n = 4). GP: germination percentage (day 5); GE: germination energy (day 2); GR: germination rate; MGT: mean germination time; VI: vigor index.

Coating Condition	GP (%)	GE (%)	GR (% Day^{-1})	MGT (Days)	Mean Total Lenght (cm)	VI (cm %)
Untreated	90 ± 8	78 ± 10	56 ± 6	1.89 ± 0.16	2.8 ± 0.4	251 ± 54
CMC	98 ± 5	83 ± 15	52 ± 5	2.05 ± 0.13	3.1 ± 0.3	303 ± 41
AlgHDA	100 ± 0	98 ± 5	77 ± 7	1.48 ± 0.17	3.7 ± 1.0	368 ± 97

The germination results indicate that the coating formulation did not adversely affect seed germination or early seedling development. On the contrary, coated seeds exhibited germination parameters comparable to, or slightly higher than, those of the untreated and CMC-coated controls. These observations suggest that the developed coating system is compatible with seed germination under the conditions evaluated. Regarding seedling growth, the mean total length and vigor index (VI) were highest for AlgHDA-treated seeds.

3.7. Evaluation of Zn-Loaded AlgHDA Coatings

Beyond its compatibility with seed germination, the ability of the AlgHDA coating to act as a carrier for functional additives was also investigated, using Zn as a model additive incorporated into the formulation as described in the Section 2. As shown in Figure 10, SEM–EDS analysis confirmed the presence of Zn in the coating layer, while no Zn signal was detected in the natural seed coat, indicating that Zn detected by EDS in the external film originated exclusively from the applied formulation.

To evaluate the transfer of Zn from the coating to the plant system, the germination assays were repeated using seeds coated with the Zn-enriched film. Following germination, the resulting seedlings were subjected to acid digestion, as described in the Section 2, and Zn content was quantified by atomic absorption spectroscopy. The seed coats, which detached naturally during germination, were excluded from the samples used for Zn determination. Seedlings obtained from uncoated seeds and from seeds coated with the Zn-free formulation were used as controls.

The Zn content measured in uncoated seedlings was 45 ± 3 μg g^{-1}, while seedlings derived from seeds coated with the Zn-free formulation showed a comparable value of 48 ± 3 μg g^{-1}. In contrast, seedlings originating from seeds coated with the Zn-enriched formulation exhibited a significant higher Zn content of 67 ± 8 μg g^{-1}. These results indicate that Zn was effectively transferred from the coating to the plant system. Moreover, since the seed coat was excluded from the analysis, the increase observed in the Zn-enriched treatment can be attributed to Zn transferred from the coating to the developing seedling tissues. These results provide a proof of concept for the ability of the developed matrix to incorporate and deliver a functional additive.

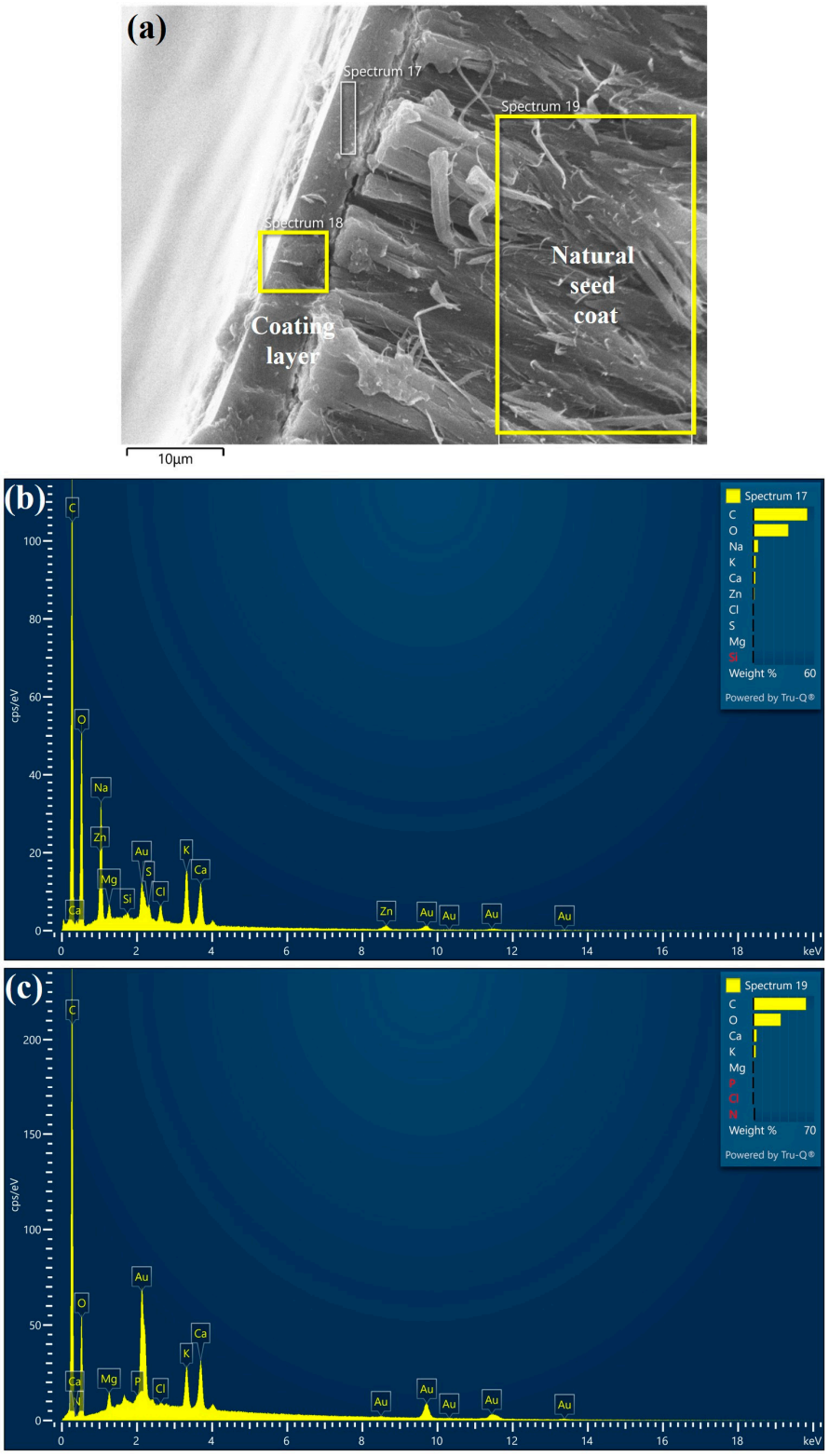


Figure 10. SEM–energy-dispersive X-ray spectroscopy (EDS) analysis of coated seeds. (**a**) SEM image showing the coating layer and natural seed coat; yellow boxes indicate representative regions selected for EDS analysis. (**b**) Representative EDS spectrum acquired from the coating layer; (**c**) representative EDS spectrum acquired from the natural seed coat.

4. Conclusions

In this manuscript, we report the synthesis and characterization of amide-modified alginate derivatives that combine aqueous processability with the ability to form water-

resistant matrices after drying. A comparison of two carbodiimide-mediated activation routes demonstrated that both synthetic approaches yield equivalent materials. Given that both reaction sequences have been reported in the literature without direct comparison within the same system, this result helps to clarify an unresolved methodological aspect of carbodiimide-mediated alginate modification and provides a reference framework for future studies employing EDC/NHS-mediated functionalization of alginate.

The modified alginates exhibited a distinctive combination of properties, including the formation of homogeneous aqueous systems after alkaline treatment and neutralization, followed by the generation of water-insoluble matrices upon drying. This behavior enables the incorporation of functional additives during processing while maintaining matrix integrity after subsequent exposure to water.

The potential of the developed derivatives as seed-coating materials was evaluated using *Vigna radiata* as a model system. All formulations successfully generated continuous coating layers on the seed surface without adversely affecting germination. Among the materials evaluated, AlgHDA showed the highest coating persistence under simulated rainfall conditions. Zn-loaded AlgHDA coatings were subsequently used as a proof of concept to demonstrate the feasibility of incorporating a micronutrient into the coating and its subsequent transfer to developing seedlings.

Overall, these results demonstrate the feasibility of generating alginate-based matrices that can be processed in aqueous media and subsequently transformed into water-insoluble films while enabling the incorporation of functional additives during formulation. This combination of properties may be attractive for the development of functional films and coatings intended to operate under humid or aqueous conditions. The seed-coating experiments presented here represent a proof of concept rather than a comprehensive evaluation of agronomic performance. Further studies involving other crop species, soil-grown plants, release kinetics, dose optimization, and greenhouse and field conditions will be required to establish the performance and applicability of these materials in agricultural settings.

Author Contributions: Conceptualization, M.I.E.; methodology, G.L., E.R. and M.I.E.; formal analysis, G.L., A.G.S. and E.R.; investigation, G.L., J.E.T., M.N., C.L., R.G.F. and A.G.S.; writing—original draft preparation, G.L., E.R. and M.I.E.; writing—review and editing, G.L., J.E.T., A.G.S., E.R. and M.I.E.; visualization, G.L. and E.R.; supervision, E.R. and M.I.E.; project administration, M.I.E.; funding acquisition, E.R. and M.I.E. All authors have read and agreed to the published version of the manuscript.

Funding: This research was financed by the Agencia Nacional de Promoción Científica y Tecnológica (PICT2020-00221), Consejo Nacional de Investigaciones Científicas y Técnicas (CONICET, PIP 2023-2025 GI-11220220100533CO), and Instituto Tecnológico de Buenos Aires (ITBA).

Data Availability Statement: The original contributions presented in this study are included in the article. In addition, the raw data supporting the findings of this study are openly available in the Repositorio Institucional de CONICET-Datos de Investigación at http://hdl.handle.net/11336/292437 (accessed on 30 August 2026).

Acknowledgments: Gabriel Lombardo has a fellowship from YPF-Tecnología (Y-TEC) and CONICET.

Conflicts of Interest: Gabriel Lombardo holds a CONICET–YPF Tecnología (Y-TEC) co-funded fellowship, awarded within the framework of a program aimed at supporting the training of early-career researchers. Gabriel Lombardo has no employment relationship or other direct financial interest in Y-TEC. Y-TEC had no role in the study design; collection, analysis, or interpretation of data; writing of the manuscript; or the decision to publish the results. The remaining authors declare no commercial or financial relationships that could be perceived as a potential conflict of interest.

References

1. Draget, K.I. Alginates. In *Handbook of Hydrocolloids*; Woodhead Publishing: Cambridge, UK, 2009; pp. 807–828.
2. Shen, K.-H.; Chiu, T.-H.; Teng, K.-C.; Yu, J.; Yeh, Y.-C. Fabrication of triple-crosslinked gelatin/alginate hydrogels for controlled release applications. *Int. J. Biol. Macromol.* **2023**, *250*, 126133. [CrossRef] [PubMed]
3. Gheorghita Puscaselu, R.; Lobiuc, A.; Dimian, M.; Covasa, M. Alginate: From Food Industry to Biomedical Applications and Management of Metabolic Disorders. *Polymers* **2020**, *12*, 2417. [CrossRef] [PubMed]
4. Yan, P.; Lan, W.; Xie, J. Modification on sodium alginate for food preservation: A review. *Trends Food Sci. Technol.* **2024**, *143*, 104217. [CrossRef]
5. Yerramathi, B.B.; Muniraj, B.A.; Donadi, J.; Bandi, K.; Kola, M. Transformation of alginate based films into food packaging material—Confines and possibilities as a renewable resource: A review. *React. Funct. Polym.* **2025**, *215*, 106358. [CrossRef]
6. Wang, N.; Wang, B.; Wan, Y.; Gao, B.; Rajput, V.D. Alginate-based composites as novel soil conditioners for sustainable applications in agriculture: A critical review. *J. Environ. Manag.* **2023**, *348*, 119133. [CrossRef] [PubMed]
7. Diestra-Balta, J.; Ponce, B.; Izquierdo-Reyna, P.; Cuneo, I.F.; Díaz-Barrera, A. Advances and technological applications of alginate hydrogels and derived formulations in agriculture: A review. *J. Agric. Food Res.* **2026**, *29*, 103029. [CrossRef]
8. Díaz Bukvic, G.; Rossi, E.; Errea, M.I. Polysaccharides as Economic and Sustainable Raw Materials for the Preparation of Adsorbents for Water Treatment. *Polysaccharides* **2023**, *4*, 219–255. [CrossRef]
9. Draget, K.I.; Skjåk-Bræk, G.; Smidsrød, O. Alginate based new materials. *Int. J. Biol. Macromol.* **1997**, *21*, 47–55. [CrossRef] [PubMed]
10. Smidsrød, O.; Skjåk-Braek, G. Alginate as immobilization matrix for cells. *Trends Biotechnol.* **1990**, *8*, 71–78. [CrossRef] [PubMed]
11. Kumar, B.; Singh, N.; Kumar, P. A review on sources, modification techniques, properties and potential applications of alginate-based modified polymers. *Eur. Polym. J.* **2024**, *213*, 113078. [CrossRef]
12. Muhammad Naqeeb Ur Rehman, Q.; Atta, R.; Muhammad Anees Ur Rehman, Q.; Muhammad Jahanzaib, J.; Maria, K.; Muhammad Asad, A.; Muhammad Shoaib, B.; Naila, F. Chemical Modifications of Alginates for Biomedical Applications-A Review. *Sci. Inq. Rev.* **2025**, *9*, 24–63. [CrossRef]
13. Wang, W.; Huang, Y.; Pan, Y.; Dabbour, M.; Dai, C.; Zhou, M.; He, R. Sodium Alginate Modifications: A Critical Review of Current Strategies and Emerging Applications. *Foods* **2025**, *14*, 3931. [CrossRef] [PubMed]
14. Taubner, T.; Marounek, M.; Synytsya, A. Preparation and characterization of amidated derivatives of alginic acid. *Int. J. Biol. Macromol.* **2017**, *103*, 202–207. [CrossRef] [PubMed]
15. Gomez, C.G.; Rinaudo, M.; Villar, M.A. Oxidation of sodium alginate and characterization of the oxidized derivatives. *Carbohydr. Polym.* **2007**, *67*, 296–304. [CrossRef]
16. Mahou, R.; Borcard, F.; Crivelli, V.; Montanari, E.; Passemard, S.; Noverraz, F.; Gerber-Lemaire, S.; Bühler, L.; Wandrey, C. Tuning the Properties of Hydrogel Microspheres by Adding Chemical Cross-linking Functionality to Sodium Alginate. *Chem. Mater.* **2015**, *27*, 4380–4389. [CrossRef]
17. Zhao, Y.; Gao, S.; Zhao, S.; Li, Y.; Cheng, L.; Li, J.; Yin, Y. Synthesis and characterization of disulfide-crosslinked alginate hydrogel scaffolds. *Mater. Sci. Eng. C* **2012**, *32*, 2153–2162. [CrossRef]
18. You, J.-O.; Rafat, M.; Auguste, D.T. Cross-Linked, Heterogeneous Colloidosomes Exhibit pH-Induced Morphogenesis. *Langmuir* **2011**, *27*, 11282–11286. [CrossRef] [PubMed]
19. Kim, Y.; Park, H.; Koo, Y. A covalently crosslinked alginate hydrogel platform with alginate oligosaccharide for tunable mechanics and enhanced antibacterial function. *Appl. Biol. Chem.* **2026**, *69*, 11. [CrossRef]
20. Lee, K.Y.; Rowley, J.A.; Eiselt, P.; Moy, E.M.; Bouhadir, K.H.; Mooney, D.J. Controlling Mechanical and Swelling Properties of Alginate Hydrogels Independently by Cross-Linker Type and Cross-Linking Density. *Macromolecules* **2000**, *33*, 4291–4294. [CrossRef]
21. Dhiman, A.; Sharma, A.K.; Bhardwaj, D.; Agrawal, G. Biodegradable dual stimuli responsive alginate based microgels for controlled agrochemicals release and soil remediation. *Int. J. Biol. Macromol.* **2023**, *228*, 323–332. [CrossRef] [PubMed]
22. Siboro, S.A.; Anugrah, D.S.; Ramesh, K.; Park, S.-H.; Kim, H.-R.; Lim, K.T. Tunable porosity of covalently crosslinked alginate-based hydrogels and its significance in drug release behavior. *Carbohydr. Polym.* **2021**, *260*, 117779. [CrossRef] [PubMed]
23. Chaudhuri, O.; Gu, L.; Klumpers, D.; Darnell, M.; Bencherif, S.A.; Weaver, J.C.; Huebsch, N.; Lee, H.-p.; Lippens, E.; Duda, G.N.; et al. Hydrogels with tunable stress relaxation regulate stem cell fate and activity. *Nat. Mater.* **2016**, *15*, 326–334. [CrossRef] [PubMed]
24. Nam, S.; Stowers, R.; Lou, J.; Xia, Y.; Chaudhuri, O. Varying PEG density to control stress relaxation in alginate-PEG hydrogels for 3D cell culture studies. *Biomaterials* **2019**, *200*, 15–24. [CrossRef] [PubMed]
25. Chhatbar, M.U.; Meena, R.; Prasad, K.; Chejara, D.R.; Siddhanta, A.K. Microwave-induced facile synthesis of water-soluble fluorogenic alginic acid derivatives. *Carbohydr. Res.* **2011**, *346*, 527–533. [CrossRef] [PubMed]
26. Wang, K.; Shang, T.; Zhao, J.; Zhang, L.; Zhou, L.; Deng, J.; Li, X.; Wang, J. A redox-sensitive coating with disulfide bonds is a promising candidate for surface-modified interventional devices. *Mater. Today Commun.* **2022**, *31*, 103380. [CrossRef]

27. Ng, Y.M.; Mat Yusuf, S.N.A.; Chiu, H.I.; Lim, V. Redox-sensitive linear and cross-linked cystamine-based polymers for colon-targeted drug delivery: Design, synthesis, and characterisation. *Pharmaceutics* **2020**, *12*, 461. [CrossRef] [PubMed]
28. Ashwinkumar, N.; Maya, S.; Jayakumar, R. Redox-responsive cystamine conjugated chitin–hyaluronic acid composite nanogels. *RSC Adv.* **2014**, *4*, 49547–49555. [CrossRef]
29. Guo, X.; Pan, Y.; Xie, Y.; Cai, P. Sodium alginate/carboxymethyl chitosan composite hydrogel beads for pH/redox dual-responsive pesticide release. *React. Funct. Polym.* **2026**, *221*, 106659. [CrossRef]
30. Honarkar, H. Waterborne polyurethanes: A review. *J. Dispers. Sci. Technol.* **2018**, *39*, 507–516. [CrossRef]
31. Arjmandi, A.; Bi, H.; Nielsen, S.U.; Dam-Johansen, K. From wet to protective: Film formation in waterborne coatings. *ACS Appl. Mater. Interfaces* **2024**, *16*, 58006–58028. [CrossRef] [PubMed]
32. Machotová, J.; Kalendová, A.; Steinerová, D.; Mácová, P.; Šlang, S.; Šňupárek, J.; Vajdák, J. Water-Resistant Latex Coatings: Tuning of Properties by Polymerizable Surfactant, Covalent Crosslinking and Nanostructured ZnO Additive. *Coatings* **2021**, *11*, 347. [CrossRef]
33. Nair, M.S.; Tomar, M.; Punia, S.; Kukula-Koch, W.; Kumar, M. Enhancing the functionality of chitosan-and alginate-based active edible coatings/films for the preservation of fruits and vegetables: A review. *Int. J. Biol. Macromol.* **2020**, *164*, 304–320. [CrossRef] [PubMed]
34. Sohail, M.; Pirzada, T.; Opperman, C.H.; Khan, S.A. Recent advances in seed coating technologies: Transitioning toward sustainable agriculture. *Green Chem.* **2022**, *24*, 6052–6085. [CrossRef]
35. Biswal, B.C.; Mishra, S.; Jaiswal, K.; Mohanty, S.; Dash, D. Seed coating innovations for sustainable horticulture enhancing germination, crop resilience and resource efficiency. *Discov. Sustain.* **2026**, *7*, 426. [CrossRef]
36. Afzal, I.; Javed, T.; Amirkhani, M.; Taylor, A.G. Modern seed technology: Seed coating delivery systems for enhancing seed and crop performance. *Agriculture* **2020**, *10*, 526. [CrossRef]
37. Haider, M.U.; Hussain, M.; Farooq, M. Optimizing zinc seed coating treatments for improving growth, productivity and grain biofortification of mungbean. *Soil Environ.* **2019**, *38*, 97. [CrossRef]
38. Cakmak, I.; Brown, P.; Colmenero-Flores, J.M.; Husted, S.; Kutman, B.Y.; Nikolic, M.; Rengel, Z.; Schmidt, S.B.; Zhao, F.-J. Chapter 7—Micronutrients. In *Marschner's Mineral Nutrition of Plants*, 4th ed.; Rengel, Z., Cakmak, I., White, P.J., Eds.; Academic Press: San Diego, CA, USA, 2023; pp. 283–385.
39. Hamzah Saleem, M.; Usman, K.; Rizwan, M.; Al Jabri, H.; Alsafran, M. Functions and strategies for enhancing zinc availability in plants for sustainable agriculture. *Front. Plant Sci.* **2022**, *13*, 1033092. [CrossRef] [PubMed]
40. Lombardo, G.; Dorm, B.C.; Salvay, A.G.; Franzi, L.; Gaffney, M.L.; Camio, J.B.P.; Trovatti, E.; Rossi, E.; Errea, M.I. Novel chitosan-based hydrogels as promising wound dressing materials with advanced properties. *Int. J. Biol. Macromol.* **2024**, *279*, 135423. [CrossRef] [PubMed]
41. Lombardo, G.; Salvay, A.G.; Pagliaricci, M.C.; D'Accorso, N.B.; Rossi, E.; Errea, M.I. Tuning the Properties of Redox-Responsive Chitosan Networks Through Diacid Chain Length and EDC–Carboxylic Acid Molar Ratio. *Polysaccharides* **2025**, *6*, 86. [CrossRef]
42. Krauland, A.H.; Guggi, D.; Bernkop-Schnürch, A. Oral insulin delivery: The potential of thiolated chitosan-insulin tablets on non-diabetic rats. *J. Control. Release* **2004**, *95*, 547–555. [CrossRef] [PubMed]
43. Rossi, E.; Ramírez, J.A.Á.; Errea, M.I. Preparation of an environmentally friendly lead adsorbent. A contribution to the rational design of heavy metal adsorbents. *J. Environ. Chem. Eng.* **2020**, *8*, 104210. [CrossRef]
44. Díaz Bukvic, G.; Ojeda Henriquez, M.; Rodríguez Vannini, A.B.; Fidalgo, M.M.; Salvay, A.G.; Rossi, E.; Errea, M.I. Impact of the Three-Dimensional Arrangements of Polyhydroxylated Crosslinkers on the Resulting Properties of Chitosan-Based Hydrogels. *Polysaccharides* **2024**, *5*, 358–379. [CrossRef]
45. Coma, M.E.; Peltzer, M.A.; Delgado, J.F.; Salvay, A.G. Water kefir grains as an innovative source of materials: Study of plasticiser content on film properties. *Eur. Polym. J.* **2019**, *120*, 109234. [CrossRef]
46. Dewi, R.; Sylvia, N.; Zulnazri, Z.; Fithra, H.; Riza, M.; Siregar, J.P.; Cionita, T.; Fitriyana, D.F.; Anis, S. The Optimization of Avocado-Seed-Starch-Based Degradable Plastic Synthesis with a Polylactic Acid (PLA) Blend Using Response Surface Methodology (RSM). *Polymers* **2024**, *16*, 2384. [CrossRef] [PubMed]
47. Kim, M.-K.; Lee, J.; Kang, A.-R. Stimuli-Responsive Hydrogels: From Swelling–Deswelling Mechanisms to Biomedical Applications. *Nanomaterials* **2026**, *16*, 329. [CrossRef] [PubMed]
48. Skrzypczak, D.; Jarzembowski, Ł.; Izydorczyk, G.; Mikula, K.; Hoppe, V.; Mielko, K.A.; Pudełko-Malik, N.; Młynarz, P.; Chojnacka, K.; Witek-Krowiak, A. Hydrogel Alginate Seed Coating as an Innovative Method for Delivering Nutrients at the Early Stages of Plant Growth. *Polymers* **2021**, *13*, 4233. [CrossRef] [PubMed]
49. Fagundes, L.K.; Nunes, U.R.; Prestes, O.D.; Fernandes, T.S.; Ludwig, E.J.; Saibt, N. Rice seed treatment and recoating with polymers: Physiological quality and retention of chemical products. *Rev. Caatinga* **2017**, *30*, 920–927. [CrossRef]
50. Ludwig, E.J.; Nunes, U.R.; Prestes, O.D.; Fagundes, L.K.; Fernandes, T.S.; Saibt, N. Polymer coating in soybean seed treatment and their relation to leaching of chemicals. *Rev. Ambiente Água* **2020**, *15*, e2602. [CrossRef]

51. Trică, B.; Tritean, N.; Constantinescu-Aruxandei, D.; Oancea, F. Optimization of the mung bean seed coating with alginate in a bottom-sprayed wurster fluidized bed coater. *Coatings* **2023**, *13*, 562. [CrossRef]
52. Onwimol, D.; Chanmprasert, W.; Changsee, P.; Rongsangchaichareon, T. Seed vigor classification using analysis of mean radicle emergence time and single counts of radicle emergence in rice (*Oryza sativa* L.) and mung bean (*Vigna radiata* (L.) Wilczek). *Agric. Nat. Resour.* **2016**, *50*, 345–350. [CrossRef]
53. Abbruzzini, T.F.; Silva, C.A.; Andrade, D.A.d.; Carneiro, W.J.d.O. Influence of digestion methods on the recovery of iron, zinc, nickel, chromium, cadmium and lead contents in 11 organic residues. *Rev. Bras. Ciência Solo* **2014**, *38*, 166–176. [CrossRef]
54. Rossi, E.; Salvay, A.G.; Errea, M.I.; Foresti, M.L. Dried water-redispersible bacterial nanocellulose with sorbitol as capping agent. *Food Hydrocoll.* **2023**, *143*, 108916. [CrossRef]
55. Gattás-Asfura, K.M.; Stabler, C.L. Chemoselective cross-linking and functionalization of alginate via Staudinger ligation. *Biomacromolecules* **2009**, *10*, 3122–3129. [CrossRef] [PubMed]
56. Leone, G.; Torricelli, P.; Chiumiento, A.; Facchini, A.; Barbucci, R. Amidic alginate hydrogel for nucleus pulposus replacement. *J. Biomed. Mater. Res. Part A* **2008**, *84A*, 391–401. [CrossRef] [PubMed]
57. Aher, N.D.; Nair, H.A. Bilayered Films Based on Novel Polymer Derivative for Improved Ocular Therapy of Gatifloxacin. *Sci. World J.* **2014**, *2014*, 297603. [CrossRef] [PubMed]
58. Alwraikat, A.; Jaradat, A.; Marji, S.M.; Bayan, M.F.; Alomari, E.; Naser, A.Y.; Alyami, M.H. Development of a Novel, Ecologically Friendly Generation of pH-Responsive Alginate Nanosensors: Synthesis, Calibration, and Characterisation. *Sensors* **2023**, *23*, 8453. [CrossRef] [PubMed]
59. Bajas, D.; Vlase, G.; Mateescu, M.; Grad, O.A.; Bunoiu, M.; Vlase, T.; Avram, C. Formulation and Characterization of Alginate-Based Membranes for the Potential Transdermal Delivery of Methotrexate. *Polymers* **2021**, *13*, 161. [CrossRef] [PubMed]
60. Zhang, X.; Chen, J.; Shao, X.; Li, H.; Jiang, Y.; Zhang, Y.; Yang, D. Structural and physical properties of alginate pretreated by high-pressure homogenization. *Polymers* **2023**, *15*, 3225. [CrossRef] [PubMed]
61. Gliko-Kabir, I.; Penhasi, A.; Rubinstein, A. Characterization of crosslinked guar by thermal analysis. *Carbohydr. Res.* **1999**, *316*, 6–13. [CrossRef]
62. Nagano, N.; Ota, M.; Nishikawa, K. Strong hydrophobic nature of cysteine residues in proteins. *FEBS Lett.* **1999**, *458*, 69–71. [CrossRef] [PubMed]
63. Zaimbashi, F.; Modiri, S.; Yari, H.; Saffari, M.; Rahimi, M. Evaluation of carboxymethyl cellulose-based seed coatings enriched with micro mineral fertilizers for enhancing wheat seed resilience to abiotic stresses. *Sci. Rep.* **2025**, *16*, 1484. [CrossRef] [PubMed]
64. Sprey, L.M.; Fernandes, T.A.; Kirillov, A.M.; Sousa, A.C. Biopolymers in seed coating for sustainable agriculture. *ACS Agric. Sci. Technol.* **2025**, *5*, 1779–1791. [CrossRef]

Disclaimer/Publisher's Note: The statements, opinions and data contained in all publications are solely those of the individual author(s) and contributor(s) and not of MDPI and/or the editor(s). MDPI and/or the editor(s) disclaim responsibility for any injury to people or property resulting from any ideas, methods, instructions or products referred to in the content.